J Mater Sci (2010) 45:2381–2389
DOI 10.1007/s10853-009-4204-2

Influence of annealing duration on the erosive wear behavior of polyphenylenesulphide composites

Taner Yilmaz

Received: 9 November 2009 / Accepted: 31 December 2009 / Published online: 14 January 2010

Abstract The influence of annealing duration on the erosive wear behavior of short glass fiber (40% w/w) and $CaCO_3$ mineral particulate (25% w/w)–short glass fiber (40% w/w) (total: 65% w/w) reinforced PPS composites has been characterized under various experimental conditions by differential scanning calorimetry (DSC) and erosion measurements. The erosive wear of the composites have been evaluated at different impingement angles (30, 45, 60, and 90°) and at four different annealing periods (30, 60, 90, and 120 min). Increase in the total crystallization causes an improvement in the erosive wear properties of the samples. Annealing time controls the morphology by influencing the degree of crystallinity in the matrix and in the fiber–matrix interface. This formation restricts fiber–matrix debonding. There is no linear proportionality between annealing time and relative degree of crystallization. The results indicate that PPS composites show maximum in wear versus impact angle relation at 60° confirming their semi-ductile failure behavior. The morphologies of eroded surface are examined by the scanning electron microscope.

Introduction

Semicrystalline engineering thermoplastics are usually reinforced with various types of organic or inorganic reinforcements like fibers or particles to form composites with improved mechanical, thermal, electrical, and chemical properties. Polyphenylenesulphide (PPS) represents a high temperature resistant, semicrystalline thermoplastic polymer with improved mechanical properties that has been mainly used as matrix material for fiber and particle reinforced composites in recent years [1].

Polyphenylenesulphide (PPS) is well studied for high temperature applications and extended periods of time. The PPS thermoplastic matrix undergoes phase transitions, such as melting and glass transition, upon heating. Such transitions affect not only the properties of polymer structure but also the features of the corresponding composites as well. Fiber-reinforced composite's performance is affected by processing conditions and subsequent thermal treatments. This performance is also affected by changing the crystallization degree and crystal orientation of the composite structure [2]. In fiber reinforced polymer composites, crystallization focused at fiber surface plays a more important role than the crystallization initiated in the matrix. During crystallization, fibers act as nucleating agents and form a transcrystalline layer, resulting in the formation of a fairly strong bonding between the fiber and the matrix [3–5]. Due to its anisotropy, the formation of transcrystallinity has a significant influence on the performance of fiber/polymer interfaces, and hence affects the mechanical and tribological properties of composites [1, 6].

Jenckel et al. [7] described transcrystallinity for the first time in 1952. Thenceforth, many researchers have joined in the investigation of transcrystallinity. Many efforts have been made to study transcrystallinity in the composites containing various matrix types and fibers under different crystallization conditions [2, 8–12]. Some researchers investigated the effect of cooling rate and methods. Huson and McGill [13] reported that rapid cooling from 215 °C to

T. Yilmaz (✉)
Civil Aviation College, Kocaeli University, Arslanbey Campus, 41285 Izmit, Turkey
e-mail: taner.yilmaz@kocaeli.edu.tr; taneryilmaz2002@yahoo.com

T. Yilmaz
Graduate School of Natural and Applied Sciences, Kocaeli University, Umuttepe Campus, 41380 Izmit, Turkey

the crystallization temperature of 138 °C facilitated the growth of transcrystallinity. Fast cooling to 170 °C followed by slow cooling to 135 °C over a period of 20 min retarded the transcrystallinity growth. Yue and Cheung [14] investigated GF with and without silane coat reinforced iPP composites and found that transcrystallinity only developed in the water quenched specimens, but specimens quenched with air-cooled and cooled in an oven preheated to 50 °C had no transcrystallinity. Avella et al. [15] investigated the effect of the crystallization temperature on the formation of transcrystallinity. Increasing crystallization temperature resulted in a change of morphology from transcrystallinity to spherulitic. The influence of annealing temperature in the melt also affected interphase properties. Auer et al. [16], Desio and Rebenfeld [17] have reported their studies of the crystallization of CF, GF, and aramid fiber reinforced PPS composites.

Tribological and structural applications of short fiber reinforced PPS composites have been increasing in engineering and aerospace applications. The fibers and the transcrystalline layer formation are very important parameters on the erosive wear behavior of PPS composite materials. PPS and its composites find increased applications in the areas where the surfaces are subjected to solid particle erosion. Solid particle erosion is a serious problem that is responsible for many failures in engineering applications. The influence of experimental related parameters (impingement angle, impact velocity, erodent type, size, shape, and hardness) and target related properties (strength, ductility, crystallinity, cross link density, reinforcement content, and arrangement) on solid particle erosion of polymers and their composites have been reviewed recently by Barkoula and Karger-Kocsis [18, 19].

In the erosion process of polymer composites that have been investigated by various researchers [20–22], factors like type of matrix, type and amount of fiber, and the interfacial bonding between fiber and matrix have important effects on the erosion behavior [23]. Investigations on the erosive wear resistance of glass fiber reinforced polymer composites showed that mechanical and tribological properties of these systems could be optimized by controlling processing conditions and cooling rate. Cooling rate controls the morphology by influencing the degree of crystallinity in the matrix and in the fiber–matrix interface. The fiber–matrix interface strength could be tailored by selecting appropriate annealing temperature–time periods [1, 5].

The detailed investigation on solid particle erosion behavior of neat PPS and its short glass fiber and mineral particulate reinforced composites has not been reported in the literature. Therefore, exhaustive and systematic study of solid particle erosion behavior of PPS and its composites is required. The main objective of this study is to investigate the influence of annealing duration on the erosive wear behavior of short glass fiber (40% w/w) and $CaCO_3$ mineral particulate (25% w/w)–short glass fiber (40% w/w) (total: 65% w/w) reinforced PPS composites under various experimental conditions.

Materials and methods

Materials

Randomly oriented short glass fiber (40% w/w) and $CaCO_3$ mineral particulate (25% w/w)–short glass fiber (40% w/w) (total: 65% w/w) reinforced PPS composites were kindly supplied by Ticona-GERMANY in form of injection molded 80 × 80 × 2 mm samples. Short glass fibers are E glass fibers having an average fiber length of 230 μm, a diameter of 10 μm. $CaCO_3$ particles used as filler, namely with the average diameter of 1.4 μm. The commercial codes of the composite plaques were 1140L6 and 6165A6, respectively. The details of PPS composites selected for the present study and their properties are listed in Table 1.

In order to promote fiber surface originated crystallinity, to form a transcrystalline layer in the in the fiber–matrix interface, the material structure should be converted to amorphous. To obtain a highly amorphous structure, samples were first heated in an oven up to 280 °C with 10 °C/min heating rate for 10 min, and then quenched (Q) in an ice-water bath. With additional heat treatment processes, it is aimed to obtain nuclei on fiber surface, and transcrystalline layer in the structure. After that the samples were annealed at 180 °C for time intervals ranging between 15 and 120 min. The samples were cooled in furnace atmosphere with 10 °C/min cooling rate down to room temperature.

Table 1 Details of the composition and properties of PPS composites

Composites	Test method	6165A6	1140L6
Density (g/cm^3)	ISO 1183	1.98	1.65
Tensile strength (MPa)	ISO 527-1,2	130	195
Tensile modulus (MPa)	ISO 527-1,2	19000	14700
Tensile elongation (%)	ISO 527-1,2	1.2	1.9
Flexural strength (MPa)	ISO 178	190	285
Flexural modulus (MPa)	ISO 178	18300	14500
Charpy impact strength (kJ/m^2)	ISO 179/1eU	20	53
Rockwell hardness (M-scale)	ISO 2039-2	100	100
Glass transition temperature (°C)	ISO 11357	110	110
Melting temperature (°C)	ISO 11357	280	280

Data on PPS composites—provided by supplier

Methods

A Mettler Toledo DSC1 (differential scanning calorimetry) was used to measure the heat of fusion of the PPS composites under nitrogen atmosphere. The analysis was carried out between 30 and 350 °C at a heating rate of 10 °C/min. 10–12 mg specimens were cut from each heat treated plaque for DSC analysis. Three specimens were tested for each type of treated samples.

The relative degree of crystallinity (percent improvement in crystallinity compared to as received sample) ($\eta\%$) was determined by DSC analysis and equations given below. In these equations, X_c, $\Delta H_{f,}$ and ΔH_f^0 are the crystalline mass fraction, the heat of fusion of a partially crystalline sample, and the heat of fusion of 100% crystalline sample, respectively, both in units of energy/mass (J/g). The value of ΔH_f^0 as reported in the literature [2, 5] for the PPS composite sample ranges from 50 to 150.4 J/g. As seen from the values, there is a large disparity. The difficulty of obtaining an accurate value of ΔH_f^0 stems from the lack of obtaining a 100% crystalline sample. Therefore, we can determine the η in proportion to that of the "as received" composites, given by Eqs. 1, 2.

$$X_c = \Delta H_f / \Delta H_f^0 \tag{1}$$

$$\eta = (X_{c,i} - X_{c,0})/X_{c,0} \times 100\% = (\Delta H_{f,i} - \Delta H_{f,0})/\Delta H_{f,0} \times 100\% \tag{2}$$

where $X_{c,i}$ and $X_{c,0}$ indicate the degree of crystallinity of annealed sample and degree of crystallinity of as received sample respectively. $\Delta H_{f,0}$ and $\Delta H_{f,i}$ are the heat of fusion of as received sample and the heat of fusion of sample after the annealing, respectively [2].

Samples prepared for erosive wear test with approximately 80 × 40 × 2 mm dimensions were cut by diamond cutter from injection molded plaques. The conditions under which erosion tests were carried out are listed in Table 2. A standard test procedure was employed for each erosion test. The samples were cleaned in acetone, dried, and weighed to an accuracy of 1×10^{-4} g using an electronic balance, eroded in the test rig for 15 s and then weighed again to determine weight loss. The ratio of this weight loss to the weight of the eroding particles causing the loss is then computed as the dimensionless incremental erosion rate.

Table 2 Erosion test parameters

Erodent	Silica sand
Erodent size (μm)	150–250
Impingement angle (°)	30, 45, 60, 90
Impact velocity (m s^{-1})	60
Erodent feed rate (g s^{-1})	9
Test temperature	RT
Nozzle to sample distance (mm)	50
Nozzle diameter (mm)	5

A schematic diagram of erosion test facility used in the present investigation is illustrated in Fig. 1. The particles are driven by a static pressure "P" of 4.5 bar and are accelerated along a 50 mm long tungsten carbide (WC) nozzle of 5 mm diameter. These accelerated particles impact the specimen, which can be held at various angles with respect to the impacting particles using an adjustable sample holder. The average velocity (v) of the silica sand at these pressures at the nozzle tip was 60 m/s. The velocity of the eroding particles is determined using a rotating disc method [24]. Erodent mass flow was measured as 9 g/s for 60 m/s impact velocity. A scanning electron micrograph of silica sand particles is shown in Fig. 2.

Results and discussion

Figure 3 shows the influence of annealing time on the crystallization of 1140L6-Q-180-30, and 1140L6-Q-180-90 coded samples between 50 and 350 °C. For example, 1140L6-Q-180-30 coded sample refers to randomly oriented short glass fiber (40% w/w) reinforced PPS sample which is quenched and annealed at 180 °C for 30 min. Both curves give a distinct primary melting endotherm (T_m) in the 285–300 °C range with a peak at 289 °C. It can be seen from Fig. 3 that the DSC scans indicate small, secondary endotherms described as T_{a1} and T_{a2}. T_{a1} is obtained approximately at 150 °C. It is seen that the position of the peak is independent of annealing conditions. Jurga et al. [25] investigated the annealing conditions of Ryton PPS R4 and indicated that these small endotherms occurred owing to melting of oligomers found in the matrix resin. These types of crystalline structures are usually obtained during the quenching process because of the kinetics of crystallization. Furthermore, Arici et al. [5] studied the influence of annealing on the performance of short glass fiber reinforced PPS composites and reported that there was not a considerable difference in the crystallinity of the samples and there was not any systematic relation between annealing conditions and total crystallinity. Despite, increase in the total crystallization caused improvement in the mechanical and tribological properties of the samples [1, 26]. On the other hand, T_{a2} was observed approximately at 20 °C above the annealing temperature similar to the studies reported in the literature [5, 27]. The T_{a2} values for 1140L6-Q-180-30 and 1140L6-Q-180-90 samples are obtained as 197 and 201 °C, respectively. As seen in Fig. 3, the crystallinity of 1140L6-Q-180-90 sample is higher than 1140L6-Q-180-30 sample. Increase in annealing time causes an increase in total crystallinity

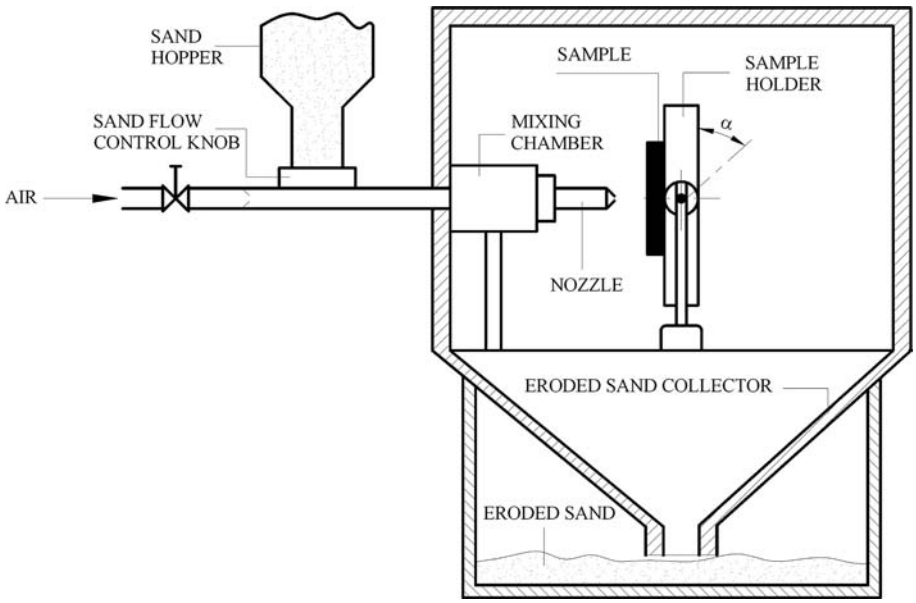

Fig. 1 Schematic diagram of erosion test rig

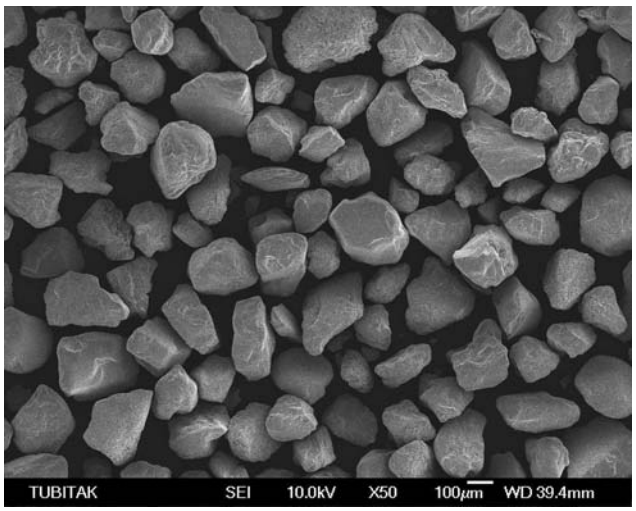

Fig. 2 Scanning electron micrograph of silica sand particles (150–250 μm)

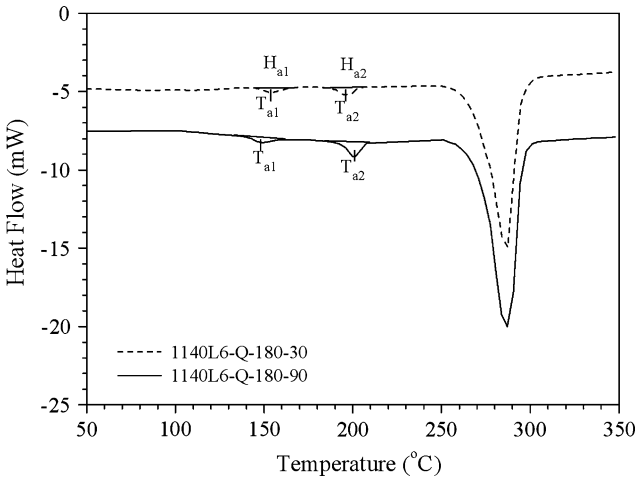

Fig. 3 Influence of annealing time on the crystallization of 1140L6 composite

degree of the composite structure. Furthermore, when the annealing time intervals are longer, it is seen that the secondary melting endotherm energy values (H_{a1} and H_{a2}) get their maximum. Primary melting endotherm energy, H_m, gets its maximum value after 90 min annealing periods.

Figure 4 illustrates the influence of annealing time on the crystallization of 6165A6-Q-180-30 and 6165A6-Q-180-90 samples. DSC scans indicate the formation of small secondary endotherms about 20 °C over the annealing temperature [1, 5, 27, 28]. As seen from Fig. 4, each DSC curve shows one secondary melting endotherm (T_{a2}). There is no formation of secondary melting endotherm (T_{a1}) that belongs to the crystals occuring at the recrystallization temperature. It has already been known that those crystals are formed during the annealing of quenched structures at above the glass transition temperature of the material. The area of the secondary endotherms increases with annealing time, indicating an increase in the total crystallinity of the composite sample.

Table 3 shows the relative crystallinity indicators as implied from heat of melting. It is seen clearly that relative crystallinity and heat of melting are increased with annealing time, but this increment continues up to 90 min annealing period. There is no liner proportionality between increasing annealing time and relative degree of crystallization. After 90-min annealing period, the maximum $\eta\%$ value is obtained.

Figure 5a, b shows the influence of annealing time, relative degree of crystallization ($\eta\%$) on erosive wear of

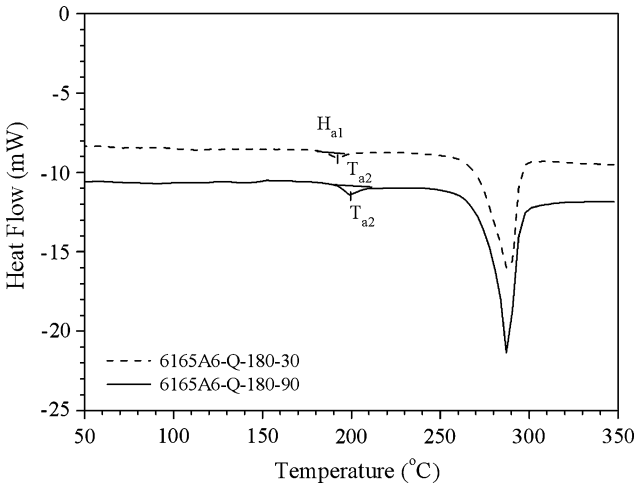

Fig. 4 Influence of annealing time on the crystallization of 6165A6 composite

Table 3 Relative crystallinity (percent improvement in crystallinity compared to as received sample) indicators as implied from heat of melting

1140L6			6165A6		
Sample code	ΔH (J g^{-1})	$\eta\%$	Sample code	ΔH (J g^{-1})	$\eta\%$
As received	21.88 ± 0.52	0	As received	15.12 ± 0.45	0
Q-180-30	23.46 ± 1.78	7.22	Q-180-30	16.09 ± 0.61	6.41
Q-180-60	24.41 ± 1.07	11.56	Q-180-60	16.73 ± 1.25	10.65
Q-180-90	25.05 ± 1.13	14.49	Q-180-90	17.25 ± 1.55	14.01
Q-180-120	23.92 ± 1.59	9.32	Q-180-120	16.37 ± 0.18	8.27

1140L6 composites with impact angles of 30° and 90° in (a) and 45° and 60° in (b), respectively. It can be seen that the weight loss was maximum at 60° impingement angle for all annealing periods. This is a semi-ductile erosion behavior. Reinforced polymeric composites have been shown to exhibit a semi-ductile behavior with maximum erosion occurring in the range of 45°–60° [29]. Annealed samples showed lower weight loss values indicating improvement in the $\eta\%$. As expected, increase in the crystallization degree resulted in the improvement of mechanical and erosive wear properties. Annealing time of 90 min showed the best erosive wear performance due to maximum $\eta\%$. This was owing to the improved fiber–matrix interface strength to the arrest of the erosive wear mechanisms like fiber/particle–matrix debonding, fiber/particle-pullout, and fiber protrusion [22].

At different impact angles (30°, 45°, and 60°) erosive wear performance is observed at different annealing periods for 6165A6 composites (Fig. 6). Also the influence of $\eta\%$ is seen. It is clear from Fig. 6 that the maximum weight loss values were obtained at impingement angle of 60° for all annealing conditions. Semi-ductile erosive wear behavior was observed. The most important parameters changing the erosive wear behavior of polymers and its composites are the impact velocity, impingement angle, the shape, size, and the hardness of selected erodent [29]. In the present study, crystallization seemed to be another important factor that influences the erosion performance.

When Figs. 5 and 6 are compared, it can be seen that weight loss values of 6165A6 composites are higher than 1140L6 composite samples. It is common for many composite manufacturers to add fillers such as powders of $CaCO_3$, carbon black, titanium white, mica flakes, glass fibers, etc. into various polymers to increase stiffness and modulus, and to reduce thermal expansion coefficients and product costs [30]. However, the above mentioned fillers are all fine and low in hardness and, thus, may not improve the wear performance [31].

Figures 7 and 8 show the influence of impingement angle and annealing period on the erosion rate of glass–fiber, glass–fiber and $CaCO_3$ particle reinforced PPS. It can be seen that the erosion rate was maximum at 60° impingement angle and minimum at 90° for both composites. This is semi-ductile erosion behavior because cutting mechanism is dominant in erosion. The erosion behavior of materials is broadly classified in the literature as ductile and brittle depending on the variation of erosion rate with impact angle. Ductile behavior is characterized by maximum erosion at low impact angles in the range of 10°–30°. On the other hand, if maximum erosion occurs at 90°, then the behavior is brittle. However, reinforced composites have been found to exhibit semi-ductile behavior with maximum erosion rate at intermediate angles typically in the range of 45°–60° [29, 32]. It can be said that a probable reason for semi-ductile behavior is the usage of the brittle short glass fibers, so that erosion is mainly caused by damage mechanisms as micro-cracking or plastic deformation due to the impact of silica sand particles.

The shapes of the curves are similar in both cases. The erosion rate was almost doubled for 6165A6 composites compared with 1140L6. Therefore, observed difference in erosion behavior of these composites should be attributed to different reinforcement or interface properties. The main reason for this formation is the influence of $CaCO_3$ particles because they are fine and low in hardness. In addition to this, mechanically weak interface between $CaCO_3$ and PPS matrix can be expressed as another reason.

As seen from Figs. 7 and 8, minimum erosion rate values are obtained at annealing period of 90 min. Annealing increases the wear performance of PPS composites because there is an increase in the total crystallinity of the system. Crystallization formed at the fiber–matrix interface plays a

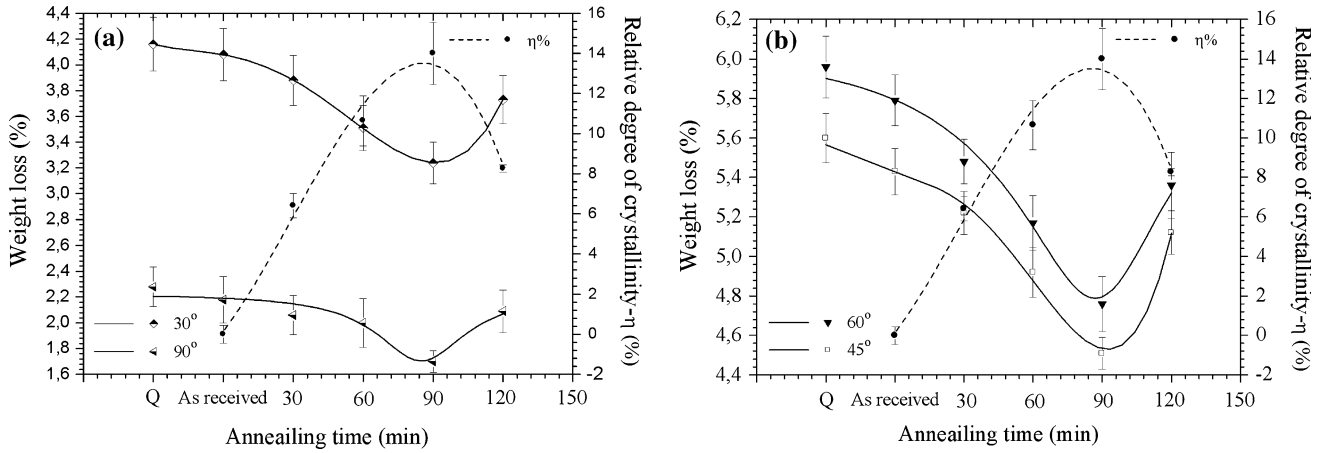

Fig. 5 Influence of annealing time, $\eta\%$ on erosive wear of 1140L6 composites with different impingement angles: **a** 30° and 90°; **b** 45° and 60°

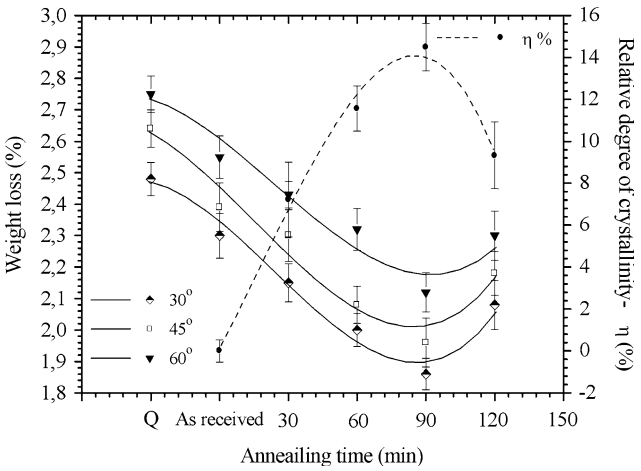

Fig. 6 Influence of annealing time, $\eta\%$ on erosive wear of 1140L6 composites with different impingement angles

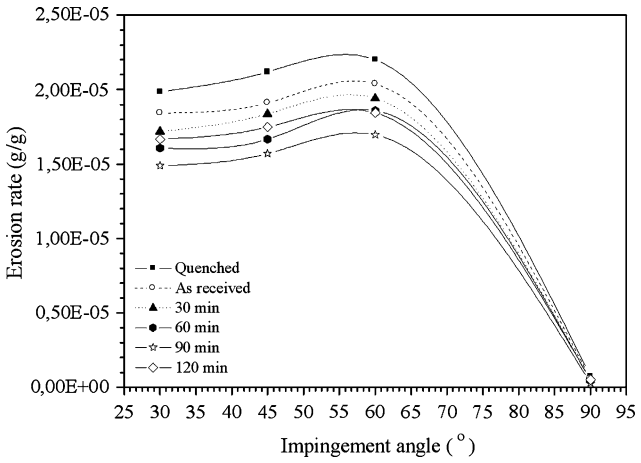

Fig. 8 Normalized erosion rate as a function of impingement angle for 1140L6 composite with different annealing periods

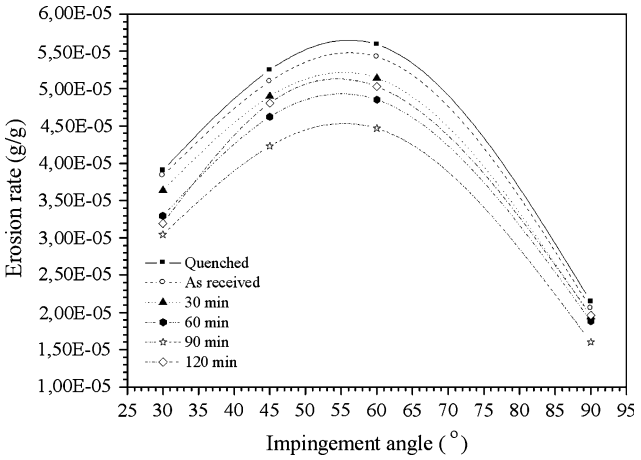

Fig. 7 Normalized erosion rate as a function of impingement angle for 6165A6 composite with different annealing periods

more important role than the crystallization formed in the matrix. Transcrystalline layer formation results in adequate bonding at the fiber–matrix interface [1].

The transcrystalline layer formation or strong interfacial bond strength prevents the pull-out and debonding of fibers and keep them to stay at polymer body. This ensures the long term stiff and rigid bodies. Transcrystallinity will almost certainly influence the mechanical properties of the interface. The presence of transcrystallinity influences the mechanical performance through its effect on fiber/matrix bonding and on the stress transfer mechanism. The transcrystalline layer formation is an additional source for stiffness and restriction of polymer chain mobility to the common factors of crystallinity and reinforcement [33].

Figure 9a, c and b, d shows micrographs of eroded surface of randomly oriented short glass fiber (40% w/w) reinforced PPS composite with annealing period of 90 min

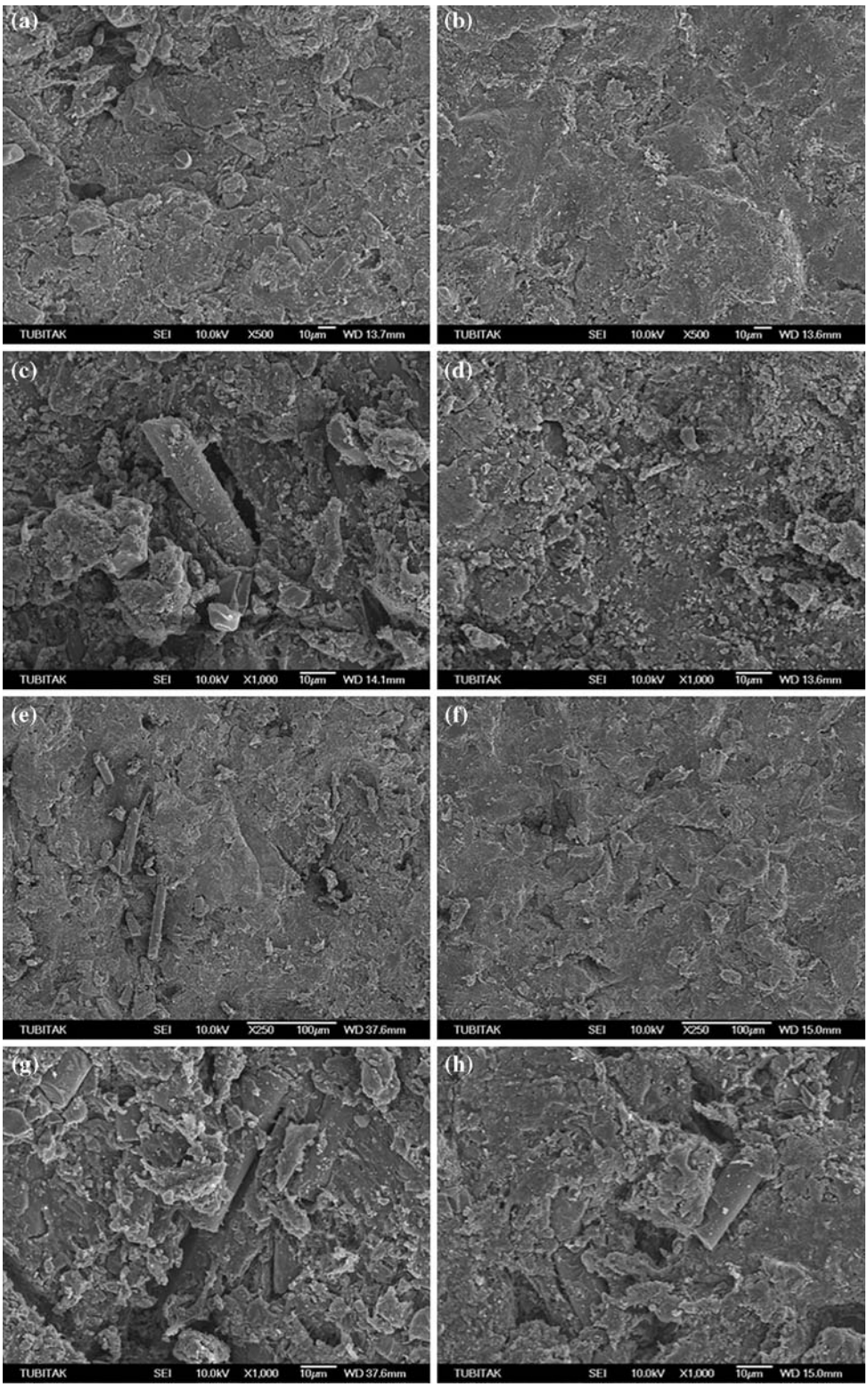

Fig. 9 Scanning electron micrographs eroded at impingement angles of 60° (**a**, **c**, **e**, **g**) and 90° (**b**, **d**, **f**, **h**) with annealing period of 90 min

at impingement angle of 60° and 90°, respectively. Repeated impact of silica sand particles caused roughening of the surface of the material. In Fig. 9a, c removal of the matrix and erosion of the fibers are clearly seen. Characteristic features of more cutting with chip formation are reflected. The matrix shows multiple fractures and material removal. The exposed fibers are broken into fragments and thus can be easily removed from the worn surfaces. Localized pit formation was also apparent on the worn surface. The observed erosion damage is characterized by

exposure of glass fibers, fiber–matrix debonding, multiple fiber cracking, and material removal. Figure 9b, d shows matrix is plastically deformed and amount of deformation is proportional to impact angle of silica sand particles. Impingement angle at 90° do not cause a higher wear loss as in the case of brittle materials due to compressive pressure at the surface. This type of pressure leads to crater formation on the worn surface; however, no material loss occurs in this mechanism.

Figure 9e, g and f, h shows SEM micrographs of eroded surface of $CaCO_3$ mineral particulate (25% w/w)–short glass fiber (40% w/w) (total: 65% w/w) reinforced PPS composite with annealing period of 90 min at impingement angle of 60° and 90°, respectively. The erosion caused by silica sand particle impacts resulted in damage to the interface between the fibers and the resin matrix. This damage was characterized by the separation and detachment of broken fibers from the resin matrix as shown in Fig. 9e, g. The observed behavior of these materials can be attributed to the following mechanism. It is well known that the fibers in composites subjected to particle flow break in bending. There is a local removal of resin material from impacted surface, which results in the exposure of the fibers. This causes intensive debonding and breakage of the fibers, which are not supported by the matrix [34]. 60° impingement angle causes not only in material removal but also in an increase in fiber/matrix debonding leading to enhanced wear. In addition to this, fiber breakage and removal of fiber debris can be seen clearly (Fig. 9e, g). Figure 9f, h shows SEM micrograph of eroded surface at impingement angle of 90°. During the normal impact, the effect of intensity of particles on target surface is less; however, exposure of fibers, fiber cracking, and breakage of the fiber can be seen from the micrograph (Fig. 9h). It is clear that during normal erosion all the available energy is dissipated by impact. There are no micro-ploughing and micro-cutting mechanisms that occurred in this process. Therefore, silica sand particles penetrate easily into the soft polymer body or cause plastic deformation and numerous crater formations in the polymer matrix.

Conclusion

Based on the experimental results, the following conclusions can be pulled out:

1. Increase in the total crystallization caused improvement in the tribological properties of the samples. The increase of annealing time causes an increase in total crystallinity degree of the composite structure. Annealed samples showed lower weight loss values indicating improvement in the $\eta\%$.
2. The weight loss values are maximum at 60° impingement angle for all annealing periods. Annealing time of 90 min shows the best erosive wear performance due to maximum $\eta\%$. In the present study, crystallization seemed to be another important factor that influences the erosion performance.
3. Weight loss values of 6165A6 composites are higher than 1140L6 composite samples. $CaCO_3$ fillers are all fine and low in hardness and, thus, may not improve the wear performance.
4. Erosion rate is maximum at 60° impingement angle and minimum at 90° for both composites. This is semi-ductile erosion behavior because cutting mechanism is dominant in erosion. That erosion is mainly caused by damage mechanisms as micro-cracking or plastic deformation due to the impact of silica sand particles.
5. The morphologies of eroded surfaces observed by SEM reveal that material removal takes place by plastic deformation, micro-cutting, and micro-cracking, exposure of fibers and removal of the fiber.

References

1. Quan H, Li ZM, Yang MB, Huang R (2005) Compos Sci Technol 65:999
2. Cao J, Chen L (2005) Polym Compos 26:713
3. Tregub A, Harel H, Marom G, Migliaresi C (1993) Compos Sci Technol 48:185
4. Incardona S, Migliaresi C, Wagner HD, Gilbert AH, Marom G (1993) Compos Sci Technol 47:43
5. Arici A, Sinmazcelik T, Capan L, Yilgor I, Yilgor E (2005) J Compos Mater 39:21
6. Harsha AP, Tewari US (2002) Polym Test 21:697
7. Jenckel K, Tcege E, Hinrichs W (1952) Kolloid-Z 129:19
8. Vendramini J, Mele P, Merle G et al (2000) J Appl Polym Sci 77:2513
9. Kenneth E, Alderson EA (2000) Adv Mater 12:617
10. He CC, Dong X, Zhang XQ et al (2004) J Appl Polym Sci 91:2980
11. Son SJ, Lee YM, Im SS (2000) J Mater Sci 35:5767. doi:10.1023/A:1004827128747
12. Nielsen AS, Pyrz R (2003) J Mater Sci 38:597. doi:10.1023/A:102186642939
13. Huson MG, McGill WJ (1984) J Polym Sci Polym Chem 22:3571
14. Yue CY, Cheung WL (1993) J Mater Sci Lett 12:1092
15. Avella M, Volpe GD, Martuscelli E et al (1992) Polym Eng Sci 32:376
16. Auer C, Kalinka G, Krause T et al (1994) J Appl Polym Sci 51:407
17. Desio GP, Rebenfeld L (1992) J Appl Polym Sci 45:2005
18. Barkoula MN, Karger-Kocsis J (2002) J Mater Sci 37:3807. doi:10.1023/A:1019633515481
19. Harsha AP, Thakre AA (2007) Wear 262:807
20. Harsha AP, Tewari US, Venkatraman B (2003) Wear 254:693
21. Rattan R, Bijwe J (2006) Mater Sci Eng A 420:342
22. Rattan R, Bijwe J (2007) Wear 262:568
23. Suresh A, Harsha AP, Ghosh MK (2008) Mater Lett 62:3246
24. Ruff AW, Ives LK (1975) Wear 35:195

25. Jurga J, Garbarczyk J, Rejeibi S, Lagodzki G, Grudzinski J (1997) In: Proceedings of international polymer seminar. Gliwice, p 377
26. Saiello S, Kenny J, Nicolais L (1990) J Mater Sci 25:3493. doi: 10.1007/BF0057537
27. Lee TH, Boey FYC, Khor KA (1995) Compos Sci Technol 53:259
28. Scobbo JJ, Hwang CR (1994) Polym Eng Sci 34:23
29. Tewari US, Harsha AP, Hager AM, Friedrich K (2003) Compos Sci Technol 63:549
30. Zhou SX, Wu LM, Sun J, Shen WD (2002) Prog Org Coat 45:33
31. Zhou R, Lu DH, Jiang YH, Li QN (2005) Wear 259:676
32. Suresh A, Harsha AP, Ghosh MK (2009) Wear 266:184
33. Sinmazcelik T, Yilmaz T (2007) Mater Des 28:641
34. Srivastava VK (2006) Mater Sci Eng A 435–436:282